Table of Contents - Supplemental Material

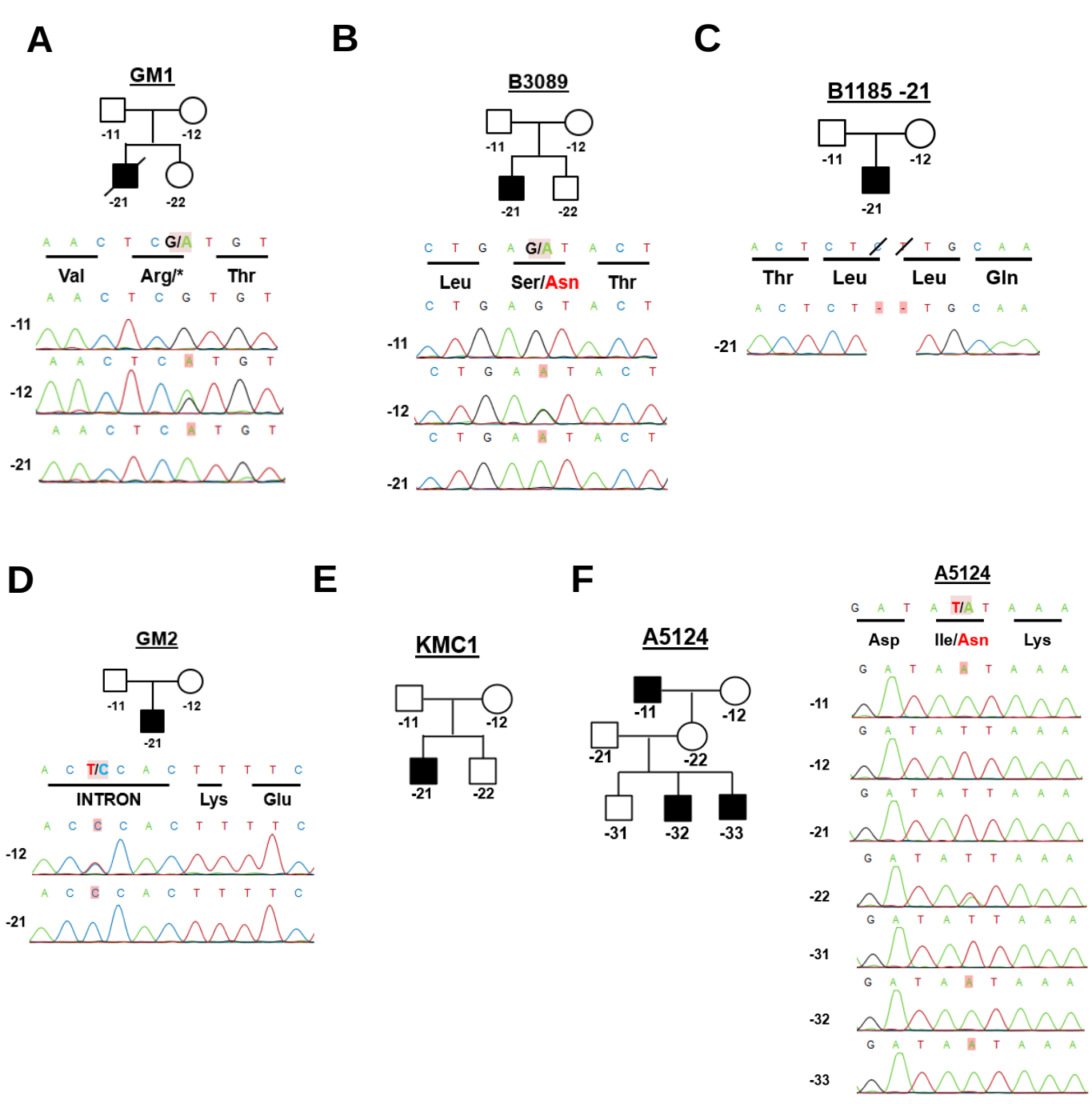

Fig. S1. Sequencing traces and family pedigrees of individuals with ARHGEF6 variants. Red colored boxes denote altered nucleotides. (A) Family GM1. (B) Family B3089. (C) Family B1185. (D) Family GM2. (E) Family KMC1, DNA was not available for Sanger confirmation but quality scores and count/coverage of exome sequencing were high. (F) Family A5124.

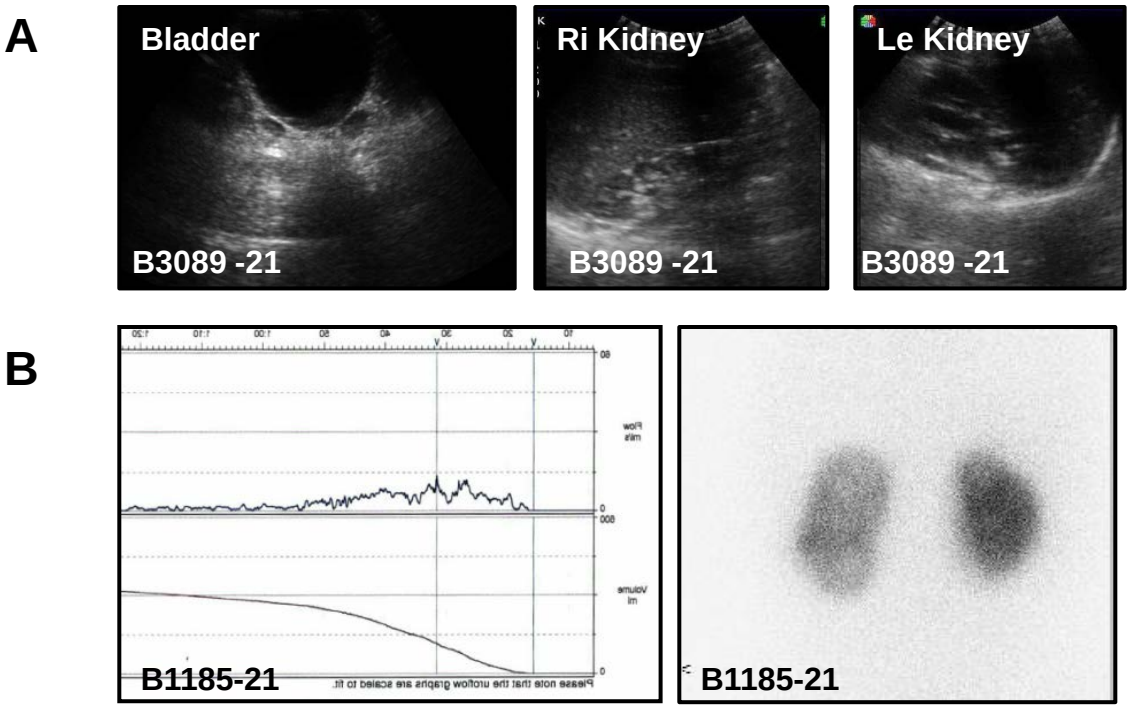

Fig. S2. Additional clinical images of individuals with ARHGEF6 variants.

(A) Clinical images of B3089. Bladder and renal ultrasound images showing bilateral dilated ureters and hypoplastic kidneys with a mild dilatation on the left.

(B) Uroflowmetry of proband B1185-21 showing obstructed voiding curve. DMSA of proband B1185 indicating an tracer uptake of 42% for the left kidney and 58% for the right kidney. Ri, right; le, left.

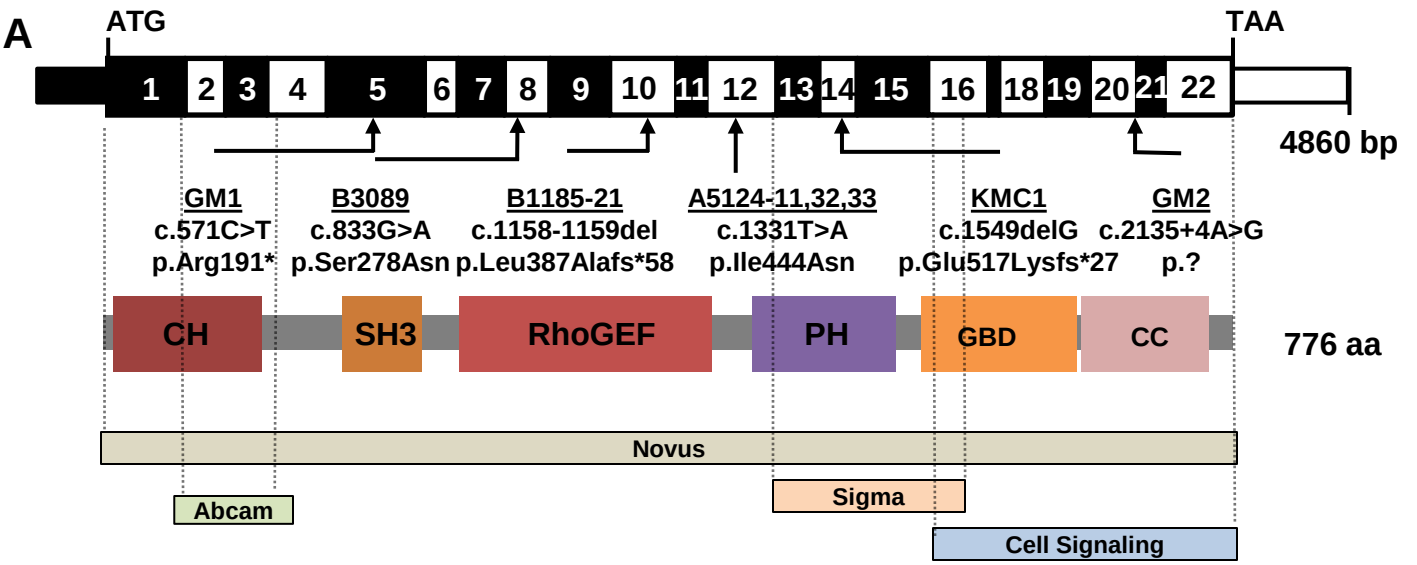

Protein	company	Company ID	Region	SP generated	Sp. Targets	Uses
ARHGEF6	Sigma	HPA003578	AA 458-600	Rabbit	Hs	WB, IF, IHC
ARHGEF6	Abcam	ab91562	AA 50-100	Rabbit	Hs	WB, IP
ARHGEF6	Novus	H00009459-B01P	AA 1-776	Mouse	Hs	WB, ELISA
ARHGEF6	Cell Signaling	4573S	C-Terminus	Rabbit	Hs, Mm, Rat	WB, IF, IHC

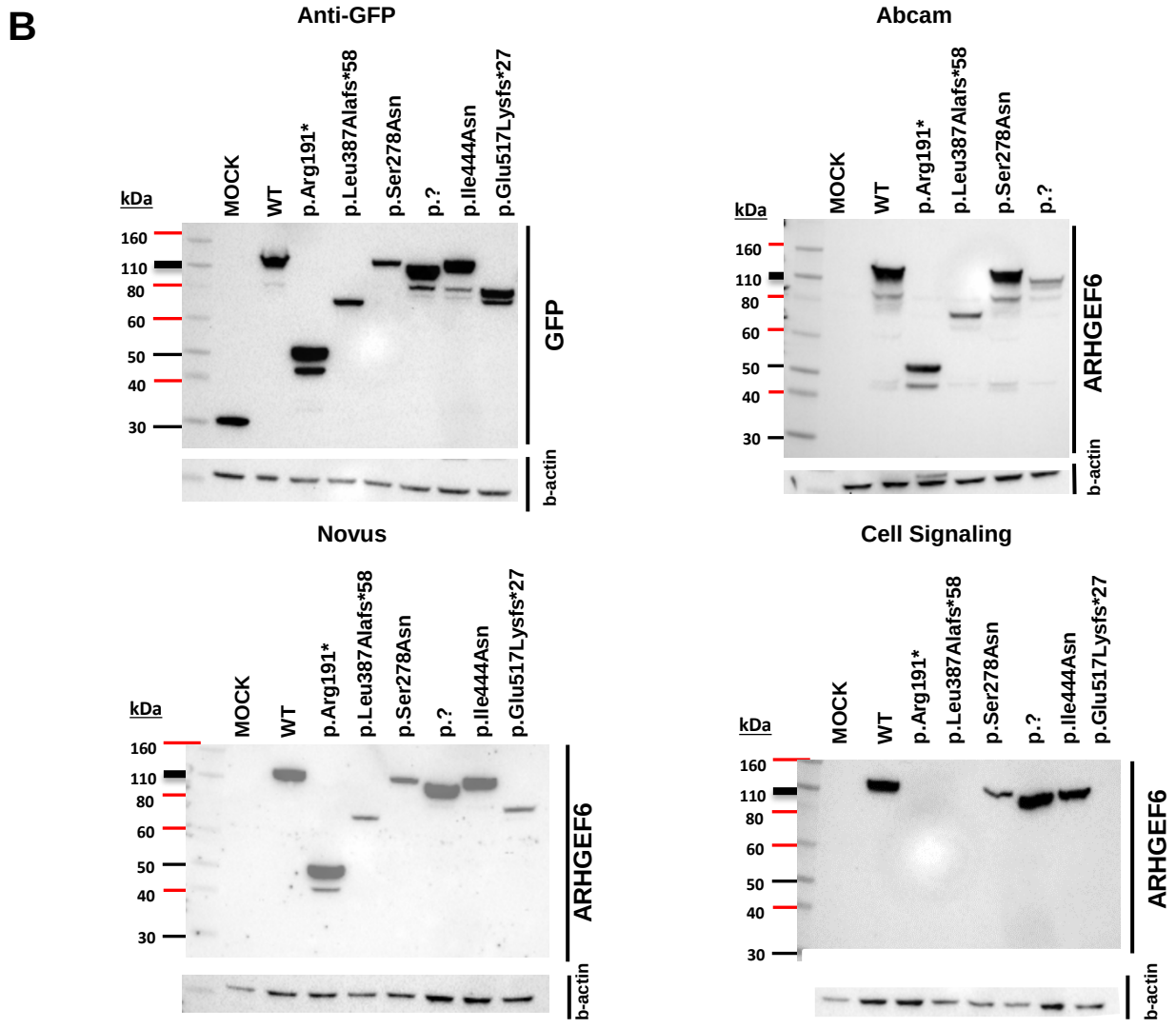

Figure S3. *ARHGEF6* cDNA clone and antibody validation.

A) Exon structure and protein domains of human *ARHGEF6* cDNA. Positions of start codon (ATG) and stop codon (TAA) are indicated. Exon numbers are marked on a black or white background. Protein domain lengths are shown by the colored boxes. Variant positions are indicated by black arrows in relation to the exon and the protein domain. Antibody scheme for ARHGEF6 showing epitopes for ARHGEF6 antibodies are indicated below protein domains and summarized in table below. Doted lines indicate epitope binding of antibody in regard to proband variants.

B) Western blot demonstrating that the ARHGEF6 antibodies identifies overexpressed N-GFP wild type and mutant cDNA in HEK293T cells at same molecular weight as anti GFP antibodies. Beta actin served as loading control. Note, that cell signaling antibody does not recognize truncating proteins.

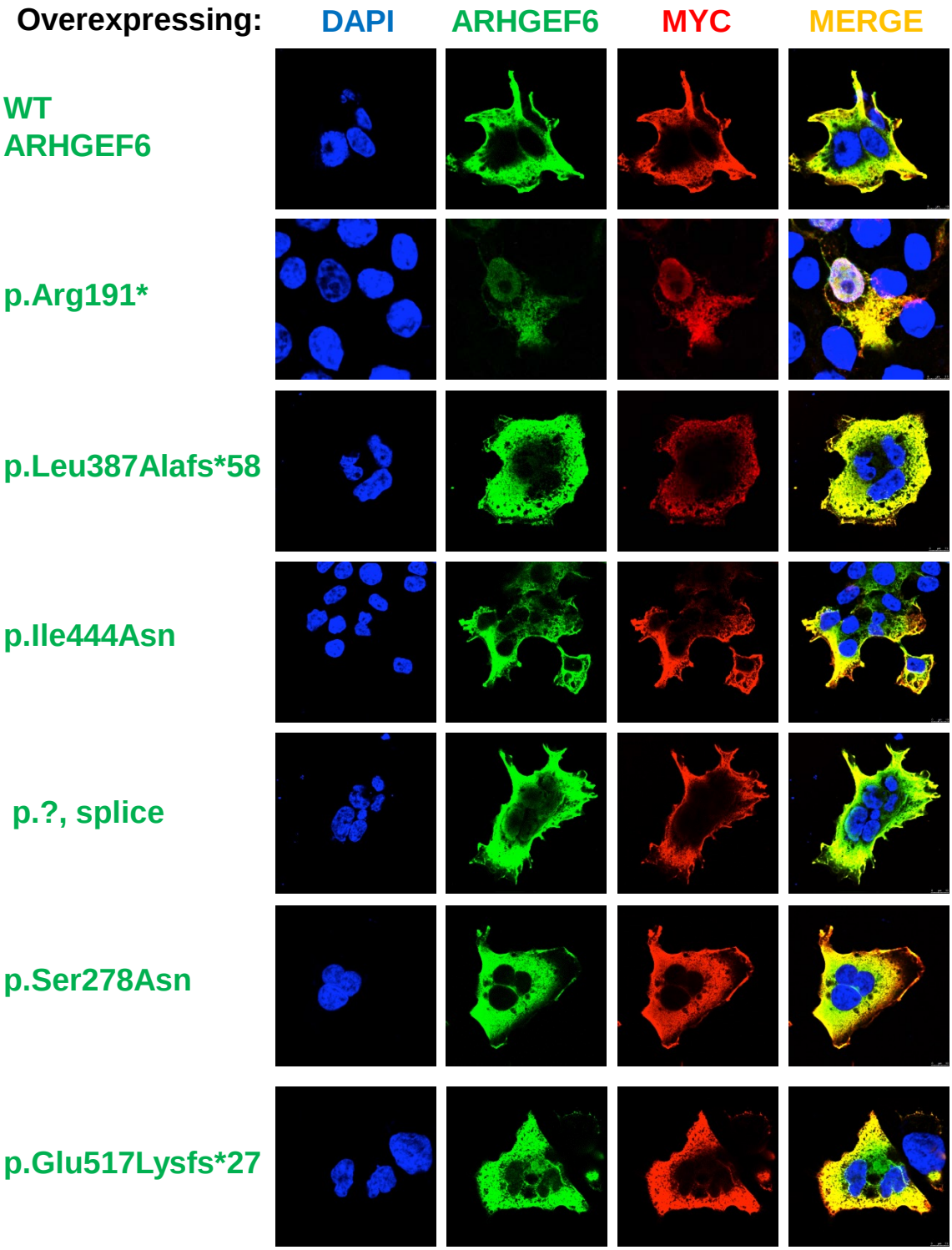

Fig. S4: ARHGEF6 antibody and clone testing on immunofluorescence.
HEK293T cells were transfected with WT vs. mutant cDNA constructs (MYC-tagged). Co-immunofluorescence of anti-MYC (DaM594) with anti ARHGEF6 (Abcam DaR488) and DAPI staining.

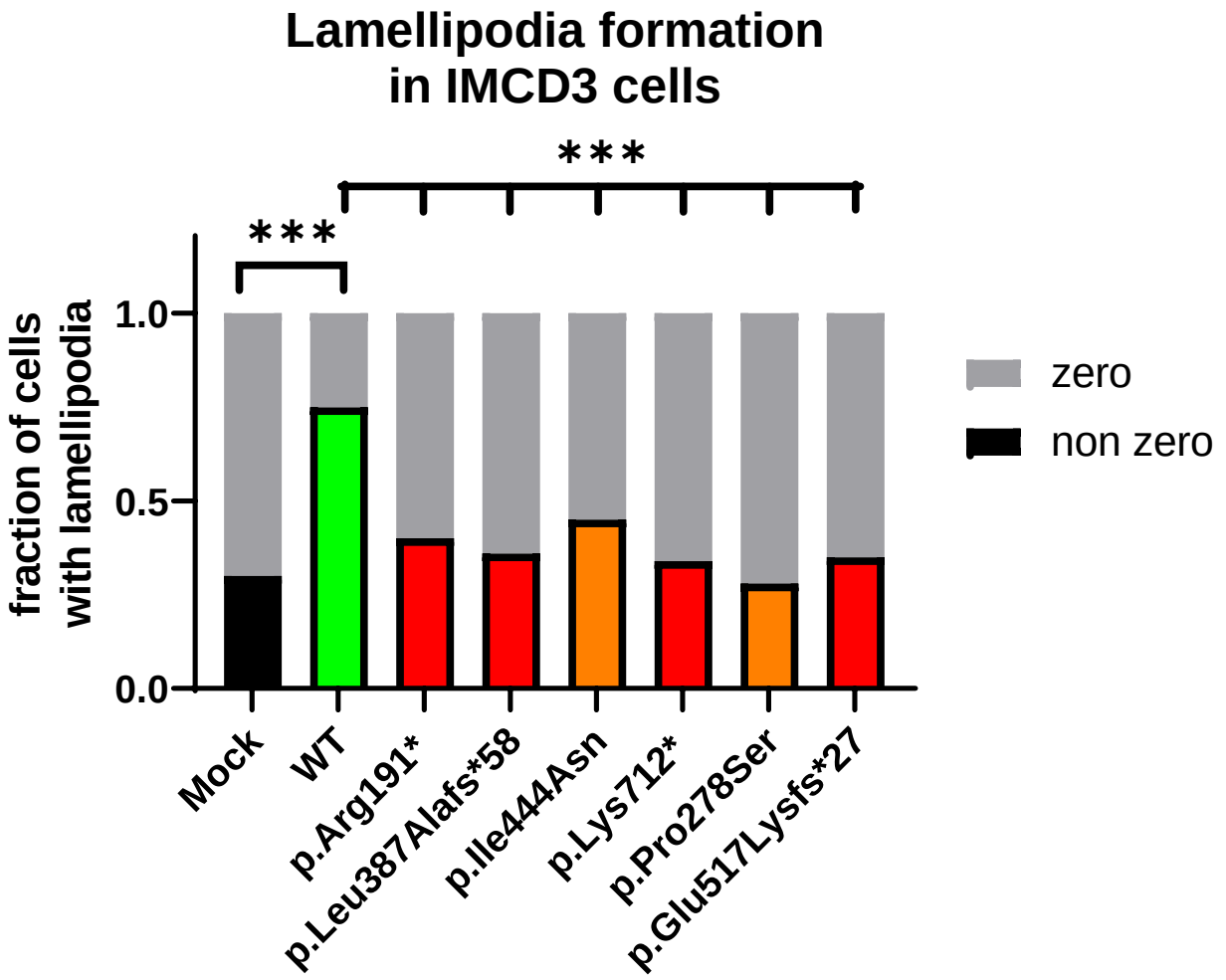

Fig. S5: ARHGEF6 WT overexpression induces lamellipodia formation in IMCD3 cells. IMCD3 cells were transfected with N-GFP *ARHGEF6* WT and mutant cDNA representing proband variants. After 24h cells were fixed and stained with phalloidin (594) labeling F-actin. Lamellipodia/membrane ruffles were counted in transfected cells in a blinded way in 3 independent experiments. Lamellipodia/membrane ruffles were defined as convex cell protrusions (~ 30 cells/group/experiment counted; total numbers: Mock n=84, WT n=113, p.Arg191* n=107, p.Leu387Alafs*58 n=106, p.Ile444Asn n=107, p.Lys712* n=94, p.Pro278Ser n=109, p.Glu517Lysfs*27 n=95). Fraction of lamellipodia-positive cells per experimental group is shown. ***, $p<0.001$, Fisher's exact test was calculated comparing WT to mock and then each of the patient variant conditions.

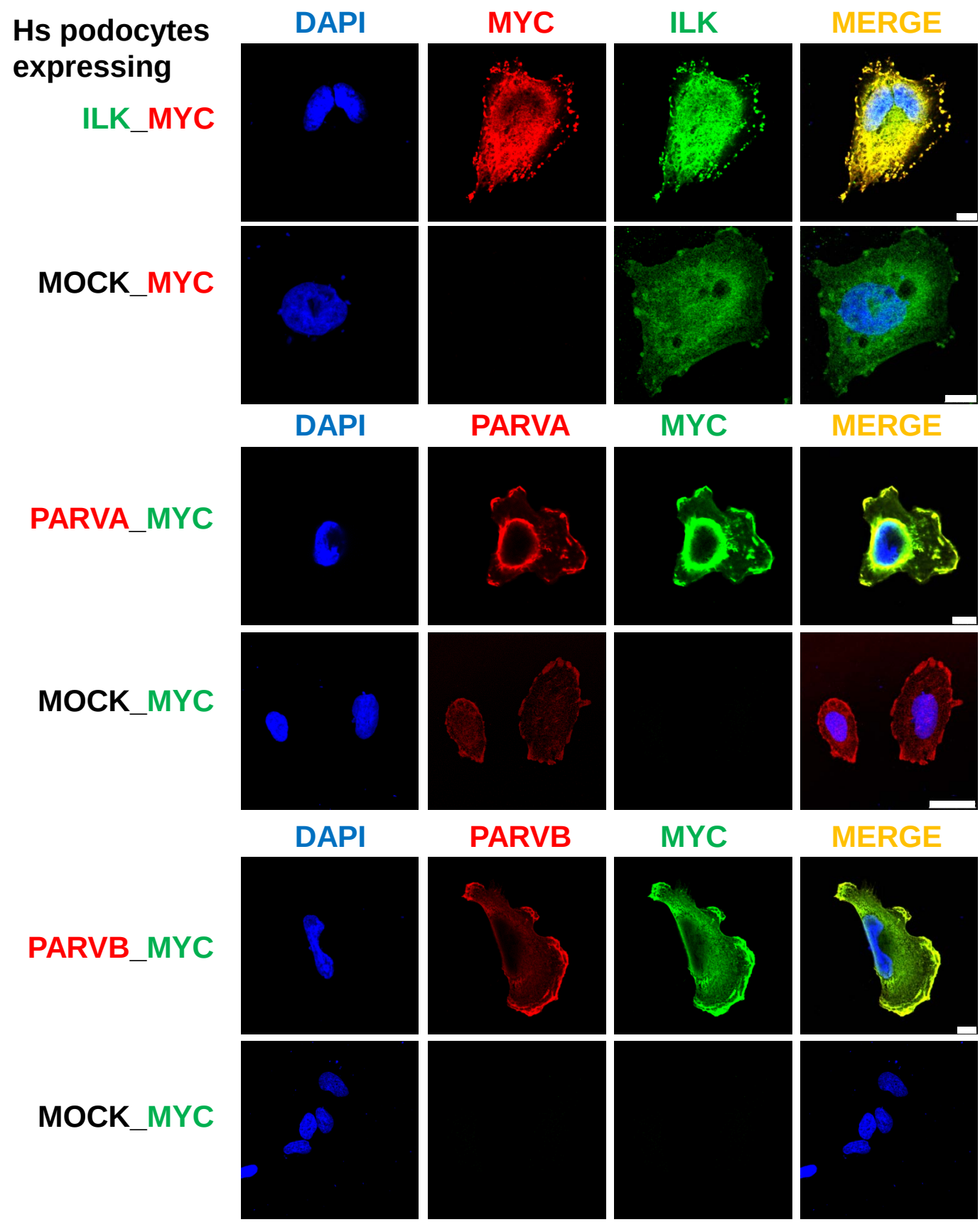

Fig. S6: Antibody and clone testing on immunofluorescence.
Human Podocytes were transfected with c-tagged *ILK*, *PARVA*, *PARVB* and MOCK_MYC cDNA constructs. Co-immunofluorescence of anti-MYC (DaM 488, DaR594) with anti ILK (Abcam, NBP2-37448, DaM488), anti PARVA (4026S Cell Signaling, DaR594), and anti PARVB (PA5-42805, Life Technology, DaR594). Scale bar 7.5 -25 µm.

A

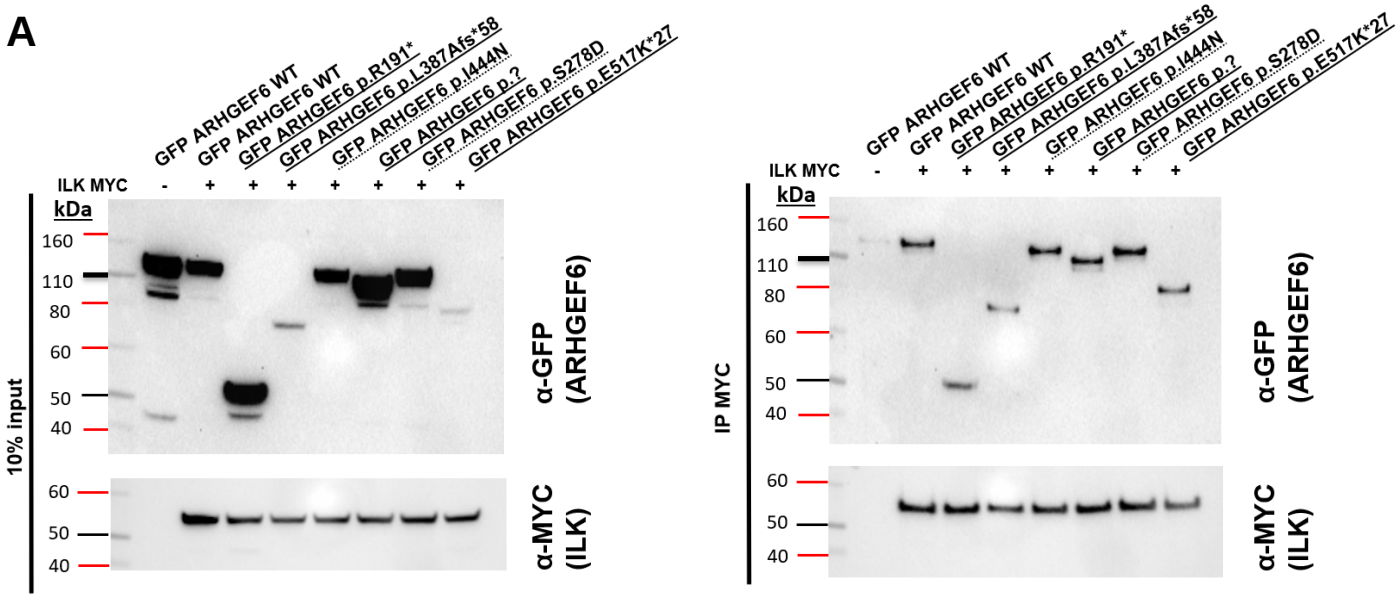

B

	IP	Input	IP corrected for Input
ARHGEF6 WT - MOCK	356	23477	0.015
ARHGEF6 WT - ILK WT	7303	16290	0.448
ARHGEF6 p.Arg191* - ILK	3921	22658	0.173
ARHGEF6 p.Leu387Alafs*58 - ILK	2343	2275	1.030
ARHGEF6 p.Ile444Asn - ILK	7576	14263	0.531
ARHGEF6 p.Lys712* - ILK	7739	30898	0.250
ARHGEF6 p.Ser278Asn - ILK	8958	19024	0.471
ARHGEF6 p.Glu517Lys*27 - ILK	4081	632	6.453

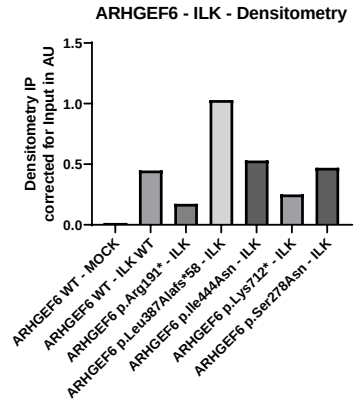

C

	IP	Input	IP corrected for Input
ARHGEF6 WT - MOCK	0	9646	0.000
ARHGEF6 WT - PARVA	3464	17416	0.199
ARHGEF6 p.Arg191* - PARVA	0	191873	0.000
ARHGEF6 p.Le387Alafs*58 - PARVA	0	18577	0.000
ARHGEF6 p.Glu517Lys*27 - PARVA	497	28085	0.018
ARHGEF6 p.Lys712* - PARVA	347	38588	0.009
ARHGEF6 p.Ile444Asn - PARVA	7554	17939	0.421
ARHGEF6 p.Ser278Asn - PARVA	2373	15545	0.153

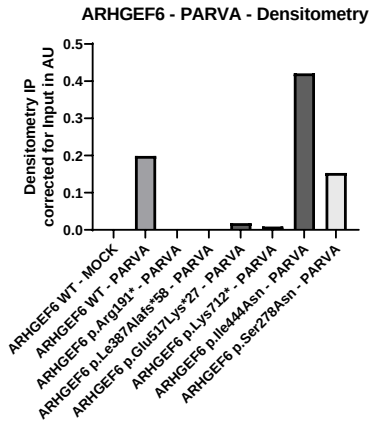

Fig. S7: ARHGEF6 interacts with ILK and PARVA. (**A**) HEK293T cells were transfected with GFP *ARHGEF6* (WT vs. proband variants) and c-MYC *ILK* cDNA constructs. Note that GFP ARHGEF6 WT and mutants co-immunoprecipitate with C-tagged ILK in HEK293T cells, but not control vector MOCK. (**B**) Table and graph show quantification of band intensities from ARHGEF6 – ILK co-immunoprecipitation assays using densitometry calculated in ImageJ. (**C**) Table and graph show quantification of band intensities from ARHGEF6 – PARVA co-immunoprecipitation assays (**Fig. 3D**) using densitometry calculated in ImageJ.

	Lumen Clearance	Laminin in Lumen	Laminin at Periphery
WT			
1	10	no	normal
2	>90	no	normal
3	10	no	normal
4	50-90	no	normal
5	10	no	normal
6	<10	no	patchy
7	50-90	low	normal
8	50-90	no	normal
9	>90	low	normal
10	50-90	no	normal
p.Arg191*			
1	10	yes	decreased
2	50-90	no	decreased
3	50-90	yes	none
4	50-90	yes	patchy
5	50-90	yes	patchy
6	<10	yes	decreased
7	>90	yes	decreased
8	50-90	yes	decreased
9	50-90	yes	patchy
10	<10	yes	none
11	50-90	yes	patchy
p.Leu387Alafs*58			
1	<10	none	none
2	90	yes	decreased
3	50-90	yes	decreased
4	50-90	none	patchy
5	90	yes	patchy, decreased
6	90	none	mostly normal
7	50-90	none	normal
8	<10	yes	abnormal
9	50-90	yes	decreased
10	90	bit	normal
p.Ile444Asn			
1	90	yes	decreased
2	50-90	yes	normal
3	50-90	yes	decreased
4	50-90	no	patchy
5	50-90	yes	patchy
6	50-90	yes	normal
7	>90	no	patchy
8	>90	yes	absent
9	10	yes	decreased
10	10	yes	decreased
11	10	yes	decreased, patchy

Fig. S8: Laminin deposition in basement membrane of MDCK cysts is affected in cells expressing proband-derived variants of *ARHGEF6*. MDCK cell 3D cultures have been used as a model for branching morphogenesis. Cells expressing either WT or proband-derived *ARHGEF6* variants (GM1, c.571C>T, p.Arg191*; B1185, c.1158_1159del, p.Leu387Alafs*58; A5124, c.1331T>A, p.Ile444Asn) were evaluated for laminin deposition as either normal or abnormal. Abnormal laminin distribution included absent staining, high luminal staining, irregular or patchy staining, or a combination of these patterns. For each *ARHGEF6* variant, cysts of all clearance categories (normal, intermediate and disorganized) were analyzed.

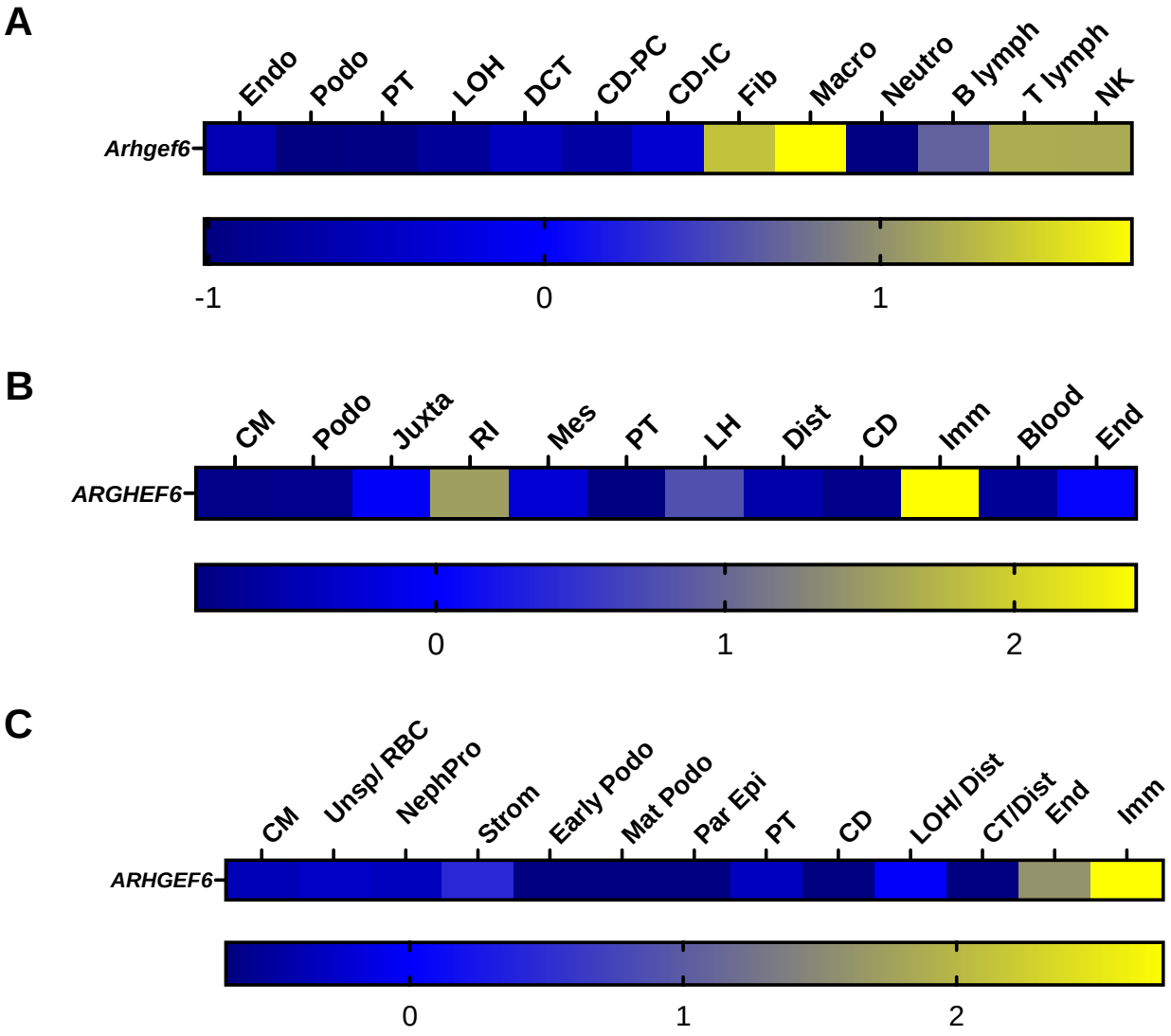

Fig. S9 Expression of *Arhgef6/ARHGEF6* in mouse and human kidney tissue based on single-cell RNA sequencing databases

Heatmaps are based on z-scores calculated from expression-positive cells per clusters for each of the publicly available single-cell RNA sequencing databases. Across all datasets, only few resident kidney cells showed *Arhgef6/ARHGEF6* expression above detection thresholds.

(A) Mouse adult kidney (**54**) 495/43,745 cells

(B) Human developmental kidney (**53**) 439/3,023 cells

(C) Human developmental kidney (**55**) 36/6,414 cells

CD, collecting duct (PC, principal cells and IC, intercalating cells); CM, cap mesenchym; DCT, distal convoluted tubule; Dist, distal tubule; Endo, endothelial cells; Fib, fibroblasts; Imm, immune cells; Juxta, juxtaglomerular cells; LH, loop of Henle; Lymph, lymphocytes; Macro, macrophages; Mes, Mesangium; NephPro, nephron progenitor cells; NK, natural killer cells; Par Epi, parietal epithelium; Podo, podocytes; PT, proximal tubule; RBC, red blood cells; RI, renal interstitium; Unspec, unspecific cell cluster

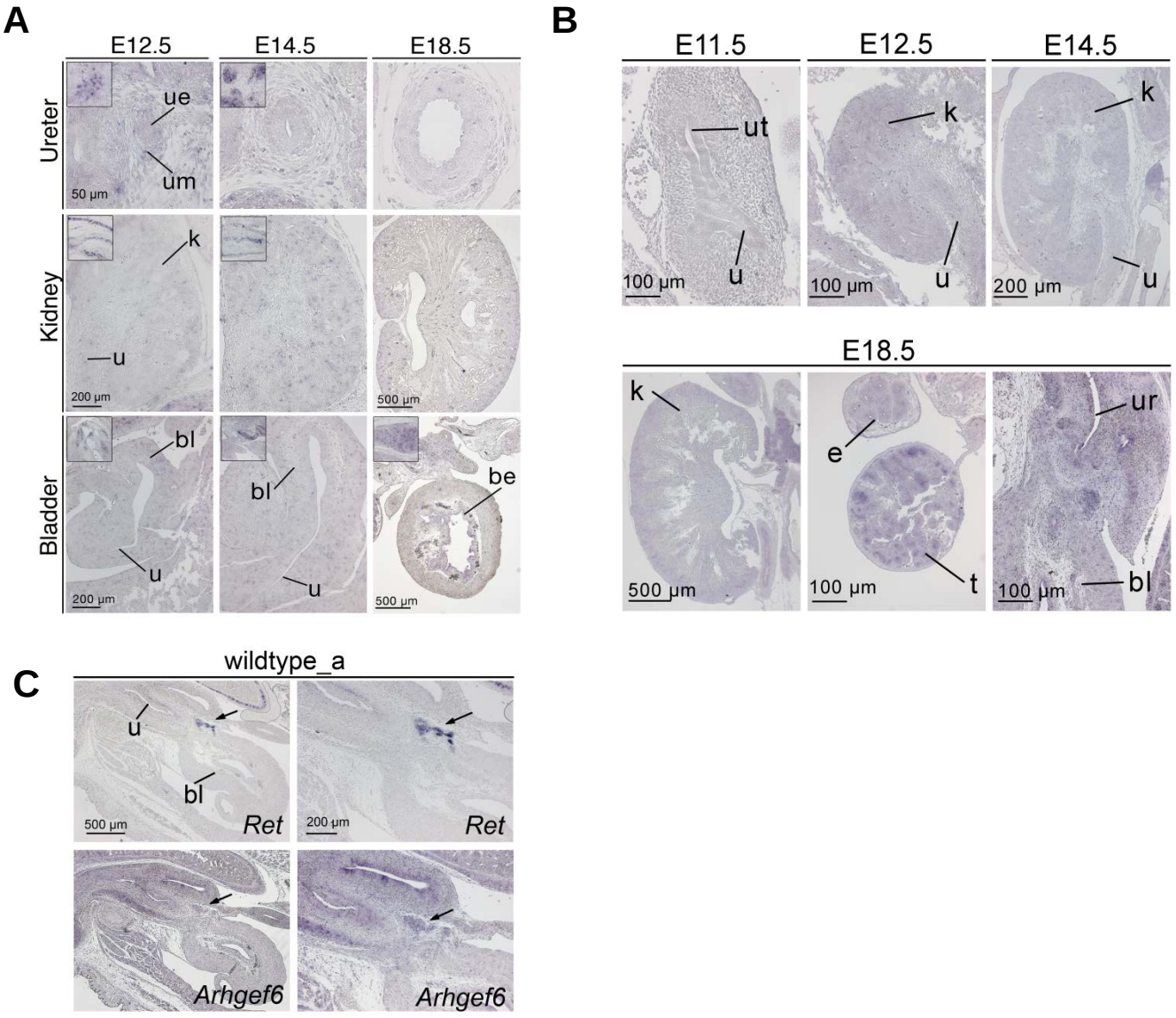

Fig. S10 Expression of *Arhgef6* in mouse urogenital development

(A-B) *In-situ* hybridization analysis of expression of *Arhgef6* in urogenital systems at different stages of embryonic development. Ue, ureteric epithelium; um, ureteric mesenchyme; gl, glomerulus; k, kidney; kc, kidney cortex; bl, bladder; u, ureter; be, bladder epithelium; t, testis.

(C) In-situ hybridization analysis of expression of *Arhgef6* next to *Ret* expression, indicating neuronal tissue. Note *Arhgef6* expression in testes and neuronal tissue surrounding the kidney/bladder and in the bladder sphincter.

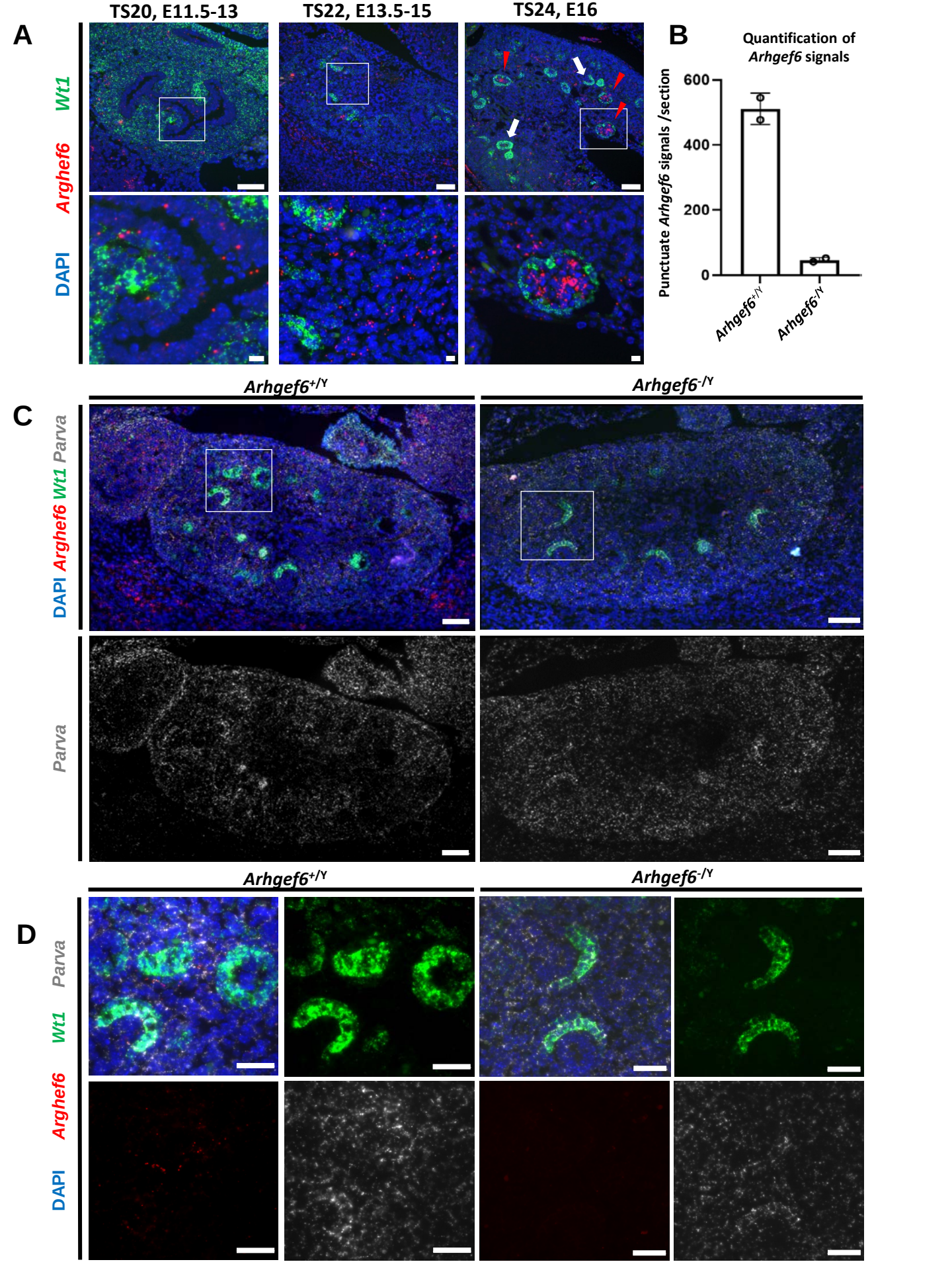
A
TS20, E11.5-13
TS22, E13.5-15
TS24, E16
Wt1
Arghef6
DAPI
B
Quantification of
Arhgef6 signals
Punctuate Arhgef6 signals /section
600
400
200
0
Arhgef6+/Y
Arhgef6-/Y
C
Arhgef6+/Y
Arhgef6-/Y
DAPI Arghef6 Wt1 Parva
Parva
D
Arhgef6+/Y
Arhgef6-/Y
Parva
Wt1
Arghef6
DAPI

Fig. S11 RNA scope-based expression of *Arhgef6* during urogenital development in WT and *Arghef6*-deficient mice

(A) Images display RNA scope analysis for *Arhgef6* expression in red and *Wt1* expression in green within urogenital systems at different stages of embryonic development. TS, Theiler stage; E, day of embryonic development; White arrows point at *Wt1*-positive structures representing early nephron structures (cap mesenchyme, renal vesicles), red arrow heads point at *Wt1*-positive structures representing later stage nephrons (immature glomerular structures); Scale bars, 100 µm and 10 µm in insets. (B) Quantification of punctuate *Arhgef6* signals in *Arhgef6*$^{+/Y}$ vs. *Arhgef6*$^{-/Y}$ kidneys. (C) Triple staining of *Wt1* (green), *Arhgef6* (red) and *Parva* (grey) probes in in *Arhgef6*$^{+/Y}$ vs. *Arhgef6*$^{-/Y}$ kidney. Scale bar, 100 µm. (D) Insets from white box shown in C are displayed with triple staining of *Wt1* (green), *Arhgef6* (red) and *Parva* (grey) probes. Scale bar, 50 µm.

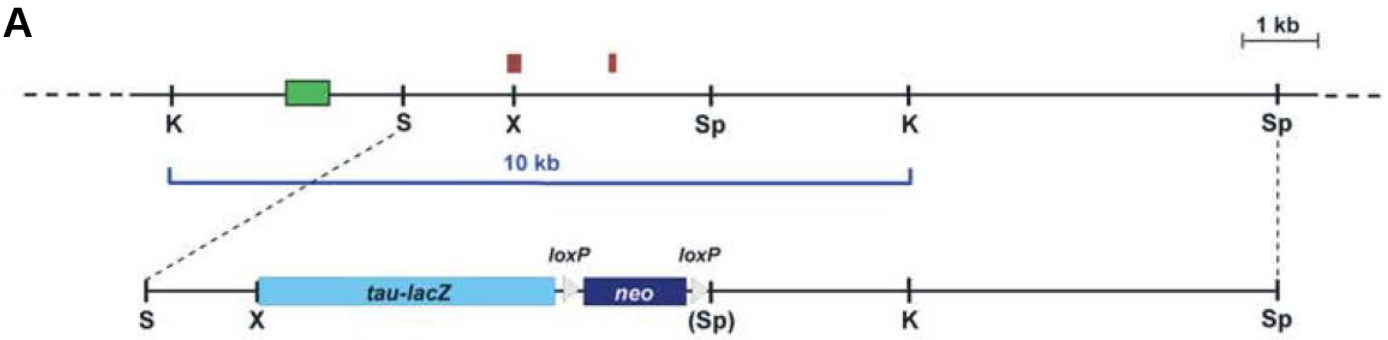

B

Total number of neonates dissected
423 (111 WT, 99 Het, 113 Hemi, 100 Hom)

Specimen extracted upon macroscopic evidence of suspected CAKUT
43 (11 WT, 7 Het, 16 Hemi, 9 Hom)

Microscopic evidence of CAKUT after Masson's trichrome staining
26 (4 WT, 5 Het, 12 Hemi, 5 Hom)

C

Macroscopic evaluation criteria:

- **Suspected duplex kidney**
- **Numeric abnormality**
- **Hydronephrosis or hydroureter**
- **Suspected hypoplasia**
- **Suspected dysplasia (side difference in color/opacity)**

Microscopic evaluation criteria:

- **Duplex kidney**
- **Hydronephrosis/hydroureter**
- **Hypodysplasia (size, cystic structures, very heterogeneous parenchyma, loss of zonal compartmentalization)**

Fig. S12: Generation and work-flow of *Arhgef6*-deficient mouse model

(A) Schematic representation of the wild-type *Arhgef6* allele (top), targeting vector (bottom) modified from Ramakers Hum. Mol. Genet. 21:268, 2011. Red boxes indicate exons 1 and 2 of *Arhgef6*, green box represents the location of the SB3 probe used for Southern blotting, light blue box the tau-lacZ gene, dark blue box the neomycin cassette and grey arrowheads loxP sites. K, KpnI; S, SphI; Sp, SpeI, (Sp), destroyed SpeI site; X, XbaI.

(B) Flow chart shows evaluation of a total of 423 neonates from matings of heterozygous *Arhgef6*$^{+/-}$ and hemizygous *Arhgef6*$^{-/Y}$ mice. In 43 out of 423 neonates CAKUT was suspected upon macroscopic evaluation. 27 out of those 43 specimens were then classified as pathologic upon Masson's trichrome staining and microscopic evaluation (Also see S.Figure 11). Table shows different CAKUT phenotypes (duplex kidneys, renal hypodysplasia, and hydronephrosis) across 224 male neonates from *Arhgef6*$^{+/-}$ x *Arhgef6*$^{-/Y}$ matings. Absolute numbers of observed CAKUT phenotypes with relative frequency in parentheses are displayed.

(C) Overview of macroscopic and microscopic criteria applied. Macroscopic criteria were used as a screening tool to identify specimen for extraction and subsequent processing for Masson's Trichrome staining. Final decision for pathology was made based on microscopic criteria. All analysis was performed in a blinded manner.

A

	Male *Arhgef6*$^{+/Y}$	Female *Arhgef6*$^{+/-}$	Male *Arhgef6*$^{-/Y}$	Female *Arhgef6*$^{-/-}$
Duplex kidney	1/111 (0.9%)	1/99 (1%)	6/113 (5.4%)	1/100 (1%)
Hypo/Dysplasia	1/111 (0.9%)	4/99 (4%)	5/113 (4.5%)	3/100 (3%)
Hydronephrosis	2/111 (1.8%)	0/99 (0%)	2/113 (1.8%)	1/100 (1%)
Any form of CAKUT (27/423)	4/111 (3.6%)	5/99 (5%)	13/113 (11.6%)	5/100 (5%)

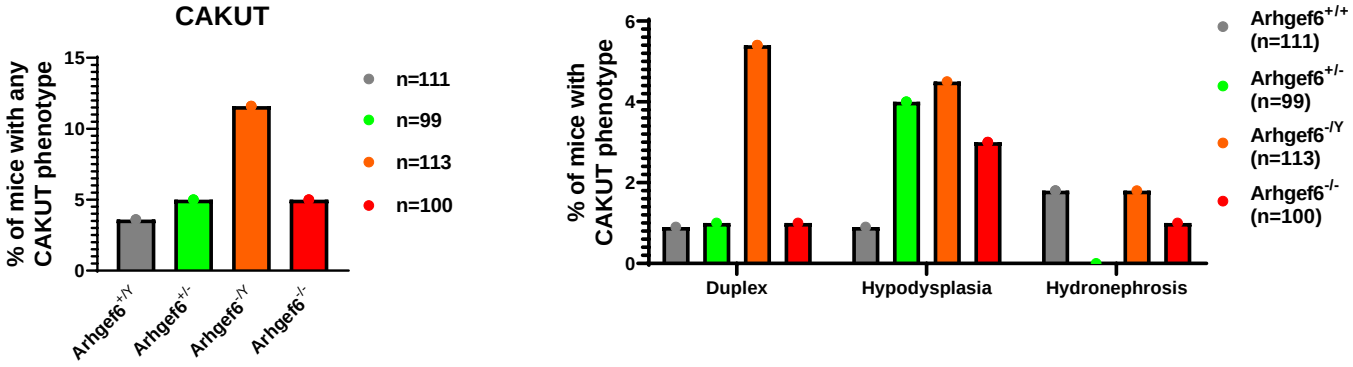

B

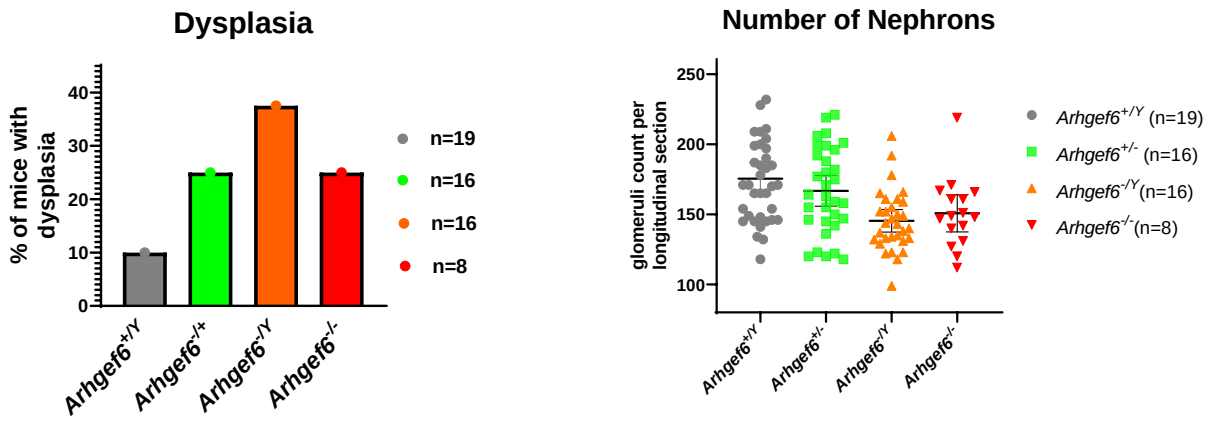

Fig. S13: CAKUT phenotype in *Arhgef6* mice (**A**) Summary of all CAKUT phenotypes and 3 sub-categories in table format and graphical representation. Heterozygous *Arhgef6*$^{+/-}$ have been mated with hemizygous *Arhgef6*$^{-/Y}$ and litters have been sacrificed at day 4 postnatally. (**B**) Evaluation of renal parenchyma from 4 week old mice of same breeding setup. Bar graph depicts percentage of mice per genotype with dysplastic features of renal parenchyma. Scatter dot plot shows number of nephrons as estimated by glomeruli per longitudinal section for each genotype. Each mouse is represented by 2 dots (1 dot per kidney). *Arhgef6*$^{+/Y}$, wildtype male; *Arhgef6*$^{+/-}$, heterozygous female; *Arhgef6*$^{-/Y}$, hemizygous male; *Arhgef6*$^{-/-}$, homozygous female; *Arhgef6*$^{+/+}$, wildtype female.

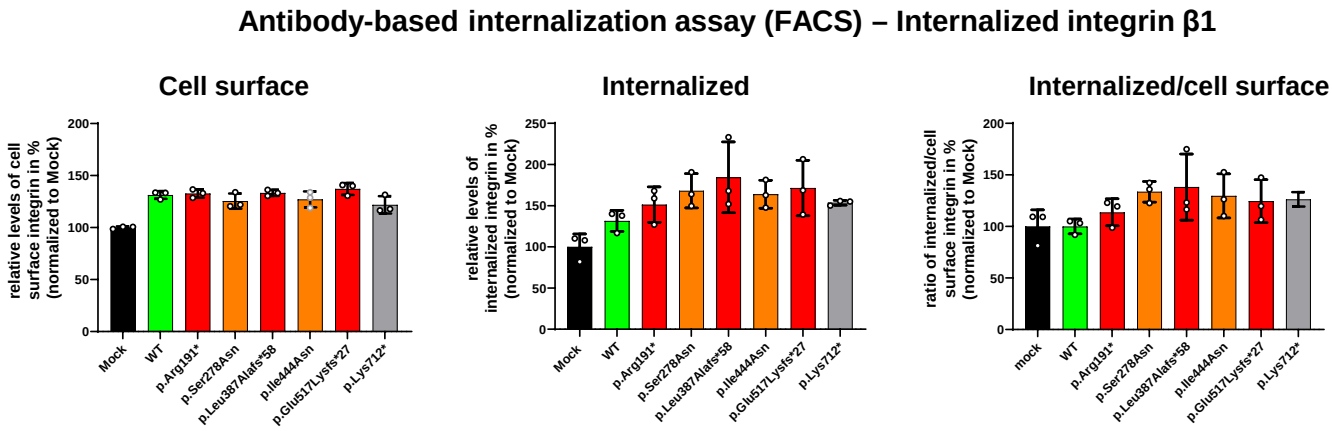

Fig. S14: Consequences of ARHGEF6 variants on β1 integrin internalization in COS7 cells

ARHGEF6 WT and proband variants were transiently expressed in COS7 cells and antibody-based integrin β1 endocytosis assays were performed. Cell surface integrin β1 was stained with Alexa Fluor 647-conjugated antibodies and internalization was induced. Amounts of both, remaining surface and internalized integrin β1 were determined by FACS analyses. Graphs show relative amounts of integrin β1 on cell surface before internalization (left), and of internalized integrin β1 after 15 minutes of internalization (middle), and of the ratio of internalized/cell surface integrin β1 (right). Each condition was normalized to the amount of integrin β1 in cells transfected with empty vector (mock). Data for three independent experiments is shown (mean ± SD).